

# Matrix Infrared Spectroscopic Studies of the $MH-C_2H_3$ and $MH_2-C_2H_2$ Intermediates in the Reactions of Ethylene with Laser-Ablated Group 5 Metal Atoms

Han-Gook Cho<sup>†</sup> and Lester Andrews<sup>\*‡</sup>

Department of Chemistry, University of Incheon, 177 Dohwa-dong, Nam-ku, Incheon, 402-749, South Korea, and Department of Chemistry, University of Virginia, Post Office Box 400319, Charlottesville, Virginia 22904-4319

Received: January 12, 2007; In Final Form: March 27, 2007

Reactions of ethylene with laser-ablated group 5 metal atoms in excess argon have been carried out during codeposition at 8 K, and the matrix infrared spectra of intermediate products have been investigated. Oxidative C–H insertion of the transition metal into a C–H bond occurs and  $\beta$ -hydrogen transfer follows to form the dihydrido complexes ( $MH_2-C_2H_2$ ). In the Ta spectra, the dihydrido complex is the primary product, whereas the Nb and V spectra reveal absorptions from both the insertion ( $MH-C_2H_3$ ) and dihydrido complexes. The insertion and dihydrido complexes identified here are in fact the reaction intermediates in the hydrogen elimination of ethylene proposed in previous reaction dynamics studies. Calculations also show that the higher oxidation-state complex becomes more stable relative to the insertion product going down the group 5 family.

## Introduction

The hydrogen abstraction reactions of hydrocarbons by vaporized transition-metal atoms have long been interesting and industrially important subjects to chemists.<sup>1</sup> In particular, reactions of ethylene with early transition-metal cations and neutral atoms have been examined carefully in a series of reaction dynamics studies.<sup>2–11</sup> The  $M-C_2H_2^+$  and  $M-C_2H_4^+$  products are monitored, and the results are explained on the basis of the reaction mechanism following the reaction path  $M + \text{ethylene} \rightarrow \pi\text{-complex} \rightarrow \text{metallacyclopropane} \rightarrow \text{insertion product} \rightarrow \text{dihydrido complex} \rightarrow M-C_2H_2 + H_2$ .<sup>12</sup>

The C–H insertion of ethylene is a key step for ultimate  $H_2$  abstraction. Activation of the C–H bond in ethylene by second-row transition metal atoms has been investigated theoretically by Siegbahn and co-workers.<sup>13</sup> They reported that the early transition metal first forms a strongly bound complex with ethylene (metallacyclopropane), which later rearranges to an insertion product. Later Parnis and co-workers<sup>3</sup> measured the reaction rate coefficients of several hydrocarbons, including ethylene, with early second-row transition metals and their neutral diatomic oxides.

While reactions of group 4 metals have been studied most,<sup>4–6,13</sup> group 5 metals are also quite efficient.<sup>6</sup> The reaction of  $V^+$  with ethylene was studied in several laboratories, and products were examined mostly with mass spectrometry<sup>6–11</sup> and theoretical calculations.<sup>13–16</sup> Recently Thompson and Parnis<sup>3b</sup> reported formation of a considerable amount of ethane along with methane in reaction of ethylene with Ti, Nb, and V atoms. They also observed two absorptions at 1552 and 1644  $cm^{-1}$  (difference of 92  $cm^{-1}$ ) in the  $V + C_2H_4$  spectra, which disappears in the process of photolysis, and tentatively assigned them to the hydrogen stretching modes of the dihydrido product ( $VH_2-C_2H_2$ ), parallel to the case of  $Ti + C_2H_4$ .

Davis and co-workers<sup>6</sup> proposed that the hydrogen elimination reaction by Nb atoms occurred mostly on the quartet potential energy surface, that the dihydrido complex was the single most stable reaction intermediate, and that there was no energy barrier between the insertion and dihydrido complexes. The Nb reaction was studied later theoretically by Sicilia and co-workers.<sup>14</sup> Similar Nb cation studies have also been performed.<sup>11,15</sup> While these studies mostly agree that the final hydrogen elimination occurs from the dihydrido reaction intermediate ( $MH_2-C_2H_2$ ),<sup>6</sup> which is formed from the insertion complex ( $MH-C_2H_3$ ), spectroscopic information on the reaction intermediates is still sketchy.

In recent investigations, the C–H insertion and dihydrido complexes from reactions of ethylene and group 4 metals are identified in their matrix infrared spectra.<sup>17,18</sup> In the Zr and Hf cases, the trihydrido complexes ( $MH_3-CCH$ ) are also observed.<sup>18</sup> Direct observation of the reaction intermediates for the hydrogen abstraction reaction of ethylene by group 5 metals would corroborate the proposed reaction path and give more insight into the reaction mechanism. In this study, the reactions of ethylene with laser-ablated group 5 metal atoms (V, Nb, and Ta) diluted in argon were carried out, and the products isolated in an argon matrix were identified by isotope substitution and density functional theory (DFT) calculations.

## Experimental and Computational Methods

Laser ablated group 5 metal atoms (Johnson-Matthey) were reacted with  $C_2H_4$ ,  $C_2D_4$ ,  $^{13}C_2H_4$  (Cambridge Isotope Laboratories, 99%), and  $CH_2CD_2$  (MSD Isotopes) in excess argon during condensation at 8 K by use of a closed-cycle He refrigerator (Air Products HC-2). The methods were previously described in detail elsewhere.<sup>19–21</sup> Concentrations of gas mixtures are typically 0.5% in argon. After reaction, infrared spectra were recorded at a resolution of 0.5  $cm^{-1}$  on a Nicolet 550 spectrometer with a mercury–cadmium–telluride (MCT) type B detector. Samples were then irradiated by a mercury arc lamp (175 W, globe removed) with a combination of optical

\* To whom correspondence should be addressed: e-mail lsa@virginia.edu.

<sup>†</sup> University of Incheon.

<sup>‡</sup> University of Virginia.

**TABLE 1: Frequencies of Product Absorptions Observed from Reactions of Ethylene with Nb in Excess Argon<sup>a</sup>**

C <sub>2</sub> H <sub>4</sub>	C <sub>2</sub> D <sub>4</sub>	<sup>13</sup> C <sub>2</sub> H <sub>4</sub>	CH <sub>2</sub> CD <sub>2</sub>	description
Dihydrido Product				
1657.3, <b>1653.5</b>	1186.5, <b>1182.0</b>	1657.3, <b>1653.5</b>	1652.7, <b>1637.1</b> , 1621.6	NbH <sub>2</sub> sym str
<b>1621.6</b> , 1618.3	<b>1169.6</b> , 1165.9	<b>1621.7</b> , 1618.3	1182.2, <b>1177.0</b> , 1169.6	NbH <sub>2</sub> str
1459.2		1413.9		C=C str
1024.8, 1021.6	<b>896.4</b> , 894.3	1006.2, 1003.2	975.2	HCCH IP bend
691.4	553.1	688.4		NbH <sub>2</sub> scis
639.9	482.8	637.9		HCCH OOP bend
609.6	516.3	596.7		NbC <sub>2</sub> str
Insertion Product				
1595.7		1595.7		Nb–H str

<sup>a</sup> All frequencies are given in reciprocal centimeters. Stronger absorptions in a set are shown in boldface type. Description is of the major coordinate.

**TABLE 2: Observed and Calculated Frequencies of the Fundamental Bands of NbH<sub>2</sub>–C<sub>2</sub>H<sub>2</sub> in the Ground <sup>2</sup>A<sub>2</sub> State<sup>a</sup>**

mode description <sup>b</sup>	NbH <sub>2</sub> –C <sub>2</sub> H <sub>2</sub>				NbD <sub>2</sub> –C <sub>2</sub> D <sub>2</sub>			NbH <sub>2</sub> – <sup>13</sup> C <sub>2</sub> H <sub>2</sub>			NbHD–C <sub>2</sub> HD		
	obs	anharm <sup>c</sup>	harm.	int	obs	harm.	int	obs	harm.	int	obs	harm.	int
A <sub>1</sub> CH str		3058.0	3208.4	0		2407.2	4		3195.6	0		3194.8	0
A <sub>1</sub> NbH <sub>2</sub> str	1653.5	1686.2	1725.2	352	1182.0	1222.6	187	1653.4	1725.1	354	1637.1	1710.1	416
A <sub>1</sub> C=C str	1459.2	1452.2	1484.3	25		1420.1	12	1413.9	1430.6	22		1452.0	18
A <sub>1</sub> HCCH IP bend		777.3	792.0	13		565.0	9		791.6	14		688.9	20
A <sub>1</sub> NbH <sub>2</sub> scis	691.4	704.6	733.5	82	553.1	601.7	40	688.4	730.7	79		663.3	62
A <sub>1</sub> NbC <sub>2</sub> str		523.1	538.5	0		460.5	7		524.3	1		512.5	17
A <sub>2</sub> HCCH OOP bend		871.3	897.4	0		723.5	0		887.1	0		834.8	11
A <sub>2</sub> NbH <sub>2</sub> twist		197.0	265.5	0		198.2	0		263.9	0		213.9	10
B <sub>1</sub> NbH <sub>2</sub> str	1621.6	1655.6	1695.6	492	1169.6	1211.2	254	1621.7	1695.6	492	1177.0	1217.7	228
B <sub>1</sub> HCCH OOP bend	639.9	650.0	639.1	80	482.8	481.3	45	637.9	635.9	79		536.3	52
B <sub>1</sub> NbH <sub>2</sub> rock		284.9	349.8	4		256.3	1		349.1	4		286.8	2
B <sub>2</sub> CH str		3029.1	3180.4	0		2338.5	0		3170.9	0		2373.2	2
B <sub>2</sub> HCCH IP bend	1021.6	1032.3	1058.3	62	896.4	914.9	22	1003.2	1039.4	64	975.2	1004.3	44
B <sub>2</sub> NbC <sub>2</sub> str	609.6	597.0	607.3	78	516.3	516.6	61	596.7	593.3	75		543.3	44
B <sub>2</sub> NbH <sub>2</sub> wag		237.5	338.4	139		244.3	72		338.0	138		309.1	94

<sup>a</sup> Frequencies are given in reciprocal centimeters; harmonic calculated intensities are in kilometers per mole. Calculations were done with B3LYP/6-311++G(3df,3pd), and the SDD core potential and basis set were used for Nb. <sup>b</sup> Mode descriptions and symmetries are for C<sub>2v</sub> structure in doublet ground state. <sup>c</sup> Calculated anharmonic frequencies.

filters for 20 min each time, were annealed, and more spectra were recorded.

Complementary DFT calculations were carried out by use of the Gaussian 03 package,<sup>22</sup> B3LYP density functional,<sup>23</sup> 6-311++G(3df,3pd) basis sets (for C, H, and V), and SDD pseudopotential and basis set<sup>24</sup> (for Nb and Ta) to provide a consistent set of vibrational frequencies for the reaction products. Additional BPW91<sup>25</sup> and MP2<sup>26</sup> calculations were done to complement the B3LYP results. Geometries were fully relaxed during optimization, and the optimized geometry was confirmed by vibrational analysis. The vibrational frequencies were calculated analytically. In the calculation of binding energy of a metal complex, the zero-point energy is included.

Anharmonic frequency calculations by numerical differentiation<sup>27</sup> (with Gaussian 03 keyword “anharmonic”) were also carried out with B3LYP to compare with experimental values and to examine the effects of anharmonicity. While the frequencies are measured in an argon matrix, which typically results in a small 1–2% red shift in the vibrational frequencies from the gas-phase values, such matrix effects were not considered in our calculations.

## Results and Discussion

Reactions of V, Nb, and Ta with ethylene isotopomers were done in condensing argon, and the observed product vibrational characteristics and their variations upon photolysis and annealing are compared with the calculated results.

**Nb + C<sub>2</sub>H<sub>4</sub>.** The IR spectra from reactions of laser-ablated Nb atoms with C<sub>2</sub>H<sub>4</sub>, C<sub>2</sub>D<sub>4</sub>, <sup>13</sup>C<sub>2</sub>H<sub>4</sub>, and CH<sub>2</sub>CD<sub>2</sub> are relatively

simple in comparison with those of group 4 metals studied previously.<sup>17,18</sup> The major product absorptions for dihydrido complex and their frequencies are listed in Table 1 and compared with calculated values in Table 2. The most prominent absorptions for the C<sub>2</sub>H<sub>4</sub> reaction are observed at 1653.5 and 1621.6 cm<sup>-1</sup> in Figure 1, which increase more than 100% upon photolysis ( $\lambda > 420$  nm) and decrease upon stepwise annealing. Strong isolated NbH<sub>2</sub> absorptions at 1610.4 and 1569.1 cm<sup>-1</sup>, first observed in the Nb and H<sub>2</sub> reaction,<sup>29</sup> are also produced here. While <sup>13</sup>C substitution leads to negligible shifts in the frequencies, as shown in Table 1, deuteration results in large shifts of –471.5 and –452.0 cm<sup>-1</sup> (Figure 2) and H/D ratios of 1.399 and 1.386 for a heavy metal hydride vibration.

The two Nb–H stretching absorptions with about 1:2 intensity ratio suggest a reaction product with two identical Nb–H bonds. The triplet patterns with CH<sub>2</sub>CD<sub>2</sub> reagent (Figure 3) verify this characterization, as the strongest intermediate bands at 1637.0 and 1176.8 cm<sup>-1</sup> are due to the NbHD derivative, the weaker 1652.7 and 1621.6 cm<sup>-1</sup> absorptions arise from NbH<sub>2</sub>–C<sub>2</sub>D<sub>2</sub>, and the weaker 1182.2 and 1169.6 cm<sup>-1</sup> bands are due to NbD<sub>2</sub>–C<sub>2</sub>H<sub>2</sub>. Important mechanistic information from this result will be discussed later. Our calculations indicate that the most plausible and stable reaction product is cyclic NbH<sub>2</sub>–C<sub>2</sub>H<sub>2</sub>. The other absorptions support formation of this dihydrido complex in the reaction of Nb with ethylene. The absorption at 1459.2 cm<sup>-1</sup> has a <sup>13</sup>C counterpart at 1413.9 cm<sup>-1</sup> (–45.3 cm<sup>-1</sup> shift and <sup>12</sup>C/<sup>13</sup>C ratio of 1.032). While the deuterium counterpart is not observed, this band is attributed to the mostly C=C stretching mode, due to the frequency and large <sup>13</sup>C shift, which

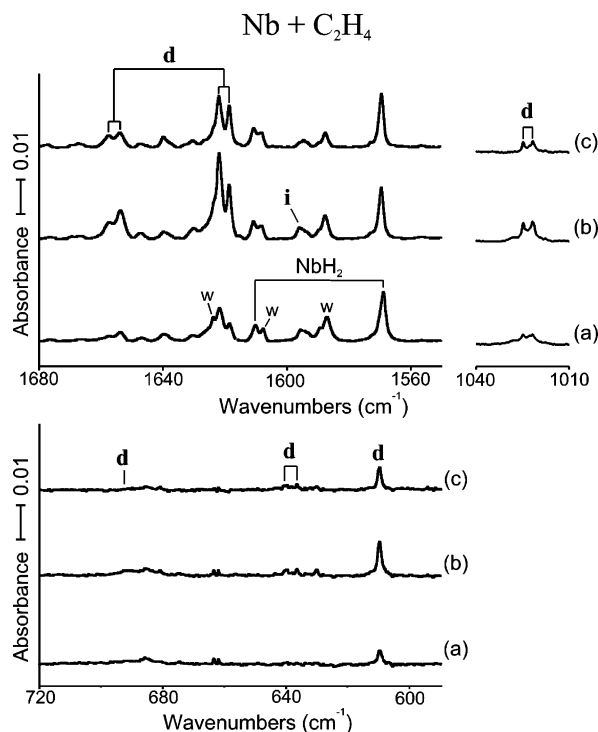


**Figure 1.** IR spectra in the regions 1680–1550, 1040–1010, and 720–590  $\text{cm}^{-1}$  for laser-ablated Nb atoms codeposited with  $\text{C}_2\text{H}_4$  in excess argon at 8 K and their variation: (a) Nb + 0.5%  $\text{C}_2\text{H}_4$  in Ar codeposited for 1 h; (b) after broad-band photolysis with  $\lambda > 420$  nm; (c) after annealing to 36 K. **d** and **i** denote the absorptions from the dihydrido and insertion products.

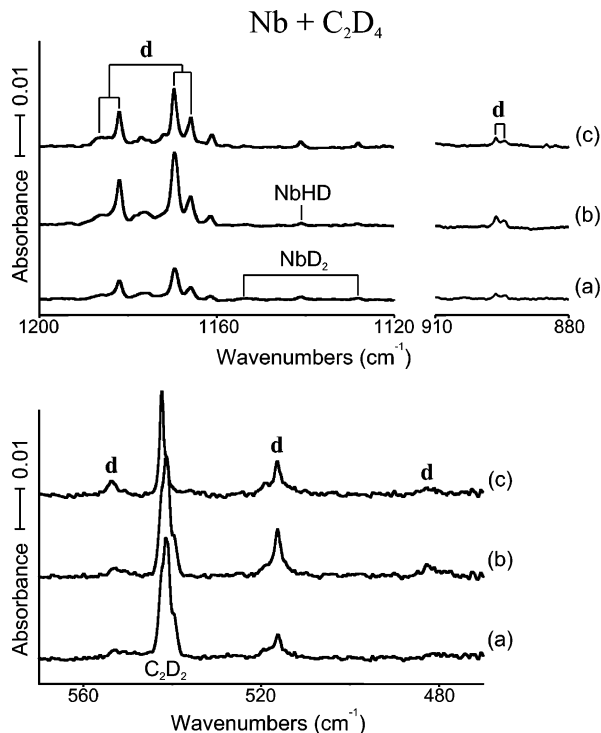


**Figure 2.** IR spectra in the regions 1200–1120, 910–880, and 570–470  $\text{cm}^{-1}$  for laser-ablated Nb atoms codeposited with  $\text{C}_2\text{D}_4$  in excess argon at 8 K and their variation: (a) Nb + 0.5%  $\text{C}_2\text{D}_4$  in Ar codeposited for 1 h; (b) after broad-band photolysis with  $\lambda > 420$  nm; (c) after annealing to 36 K. **d** denotes the dihydrido product absorption.

is not IR-active in ethylene itself. Another absorption at 1021.6  $\text{cm}^{-1}$  has its D and  $^{13}\text{C}$  counterparts at 896.4 and 1003.2  $\text{cm}^{-1}$

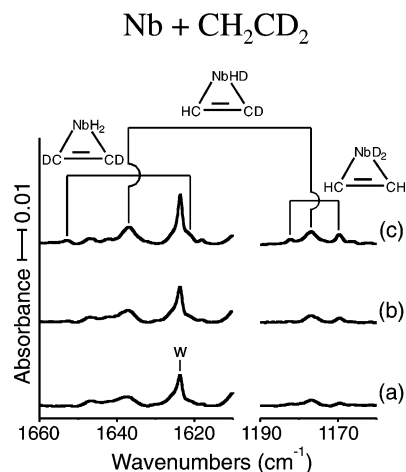


**Figure 3.** IR spectra in the regions 1660–1610 and 1190–1160  $\text{cm}^{-1}$  for laser-ablated Nb atoms codeposited with  $\text{CH}_2\text{CD}_2$  in excess argon at 8 K and their variation: (a) Nb + 0.5%  $\text{CH}_2\text{CD}_2$  in Ar codeposited for 1 h; (b) after broad-band photolysis with  $\lambda > 420$  nm; (c) after full arc irradiation.

(H/D and  $^{12}\text{C}/^{13}\text{C}$  ratios of 1.140 and 1.018), respectively. This band is assigned to the HCCH in-plane bending mode on the basis of the frequency and substantial magnitude of D shift.

The weak absorption at 691.4  $\text{cm}^{-1}$  showing a large D shift of  $-138.3$   $\text{cm}^{-1}$  but a small  $^{13}\text{C}$  shift of  $-3.0$   $\text{cm}^{-1}$  (H/D and  $^{12}\text{C}/^{13}\text{C}$  ratios of 1.250 and 1.004), which is compared to calculated shifts of  $-131.8$  and  $-2.8$   $\text{cm}^{-1}$ , most probably arises from the  $\text{NbH}_2$  scissoring mode. On the further low-frequency side, the absorption at 639.9  $\text{cm}^{-1}$  also shows large D and small  $^{13}\text{C}$  shifts of  $-157.1$  and  $-2.0$   $\text{cm}^{-1}$  (H/D and  $^{12}\text{C}/^{13}\text{C}$  ratios of 1.325 and 1.003), respectively, and they are compared with the calculated frequency shifts of  $-156.3$  and  $-3.2$   $\text{cm}^{-1}$ . This band is assigned to the HCCH out-of-plane bending mode. The relatively strong absorption at 609.6  $\text{cm}^{-1}$  has its D and  $^{13}\text{C}$  counterparts at 516.3 and 596.7  $\text{cm}^{-1}$  (D and  $^{13}\text{C}$  shifts of  $-93.3$  and  $-12.9$   $\text{cm}^{-1}$ , compared with the calculated shifts of  $-90.7$  and  $-14.0$   $\text{cm}^{-1}$ ), respectively. It is attributed to the Nb–C<sub>2</sub> stretching mode.

As shown in Table 2, there is a good match between the observed frequencies and the B3LYP-calculated values for  $\text{NbH}_2\text{--C}_2\text{H}_2$  in the doublet ground state ( $^2A_2$ ). The frequencies calculated with anharmonic correction are of course closer to the observed values than the harmonic frequencies. However, in the case of lower frequency modes that often involve interactions with other modes, the anharmonic potential function is more difficult to define mathematically, and such frequency calculations are not as reliable (the  $\text{NbH}_2$  wag, for example). Similar harmonic frequencies were predicted by the BPW91 ( $-22$  and  $-19$   $\text{cm}^{-1}$  for Nb–H modes) and the MP2 ( $+59$  and  $+57$   $\text{cm}^{-1}$  for Nb–H modes) methods. The differences between calculated and observed frequencies are typical for these calculations.<sup>30</sup> This confirms that oxidative insertion by Nb atoms into the C–H bond and following hydrogen migration occur during codeposition and particularly visible photolysis ( $\lambda > 420$  nm) afterward.

The observation of stronger NbHD–CHCD and weaker  $\text{NbH}_2\text{--C}_2\text{D}_2$  and  $\text{NbD}_2\text{--C}_2\text{H}_2$  absorptions with  $\text{CH}_2\text{CD}_2$  verifies that transfer of the nearer  $\beta$ -hydrogen to the Nb center takes place [in the first insertion product computed structure, the  $\beta$ -H to Nb distance is 2.207 Å, and the  $\alpha$ -H to Nb distance is 3.051 Å]. Notice that the Nb–H(D) stretching frequencies for the mixed isotopic products are very nearly the same as for the pure isotopic species, as verified by calculations. The formation of

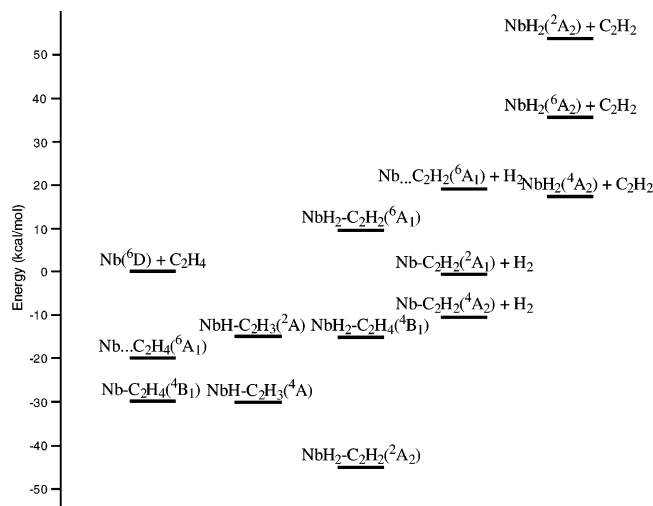


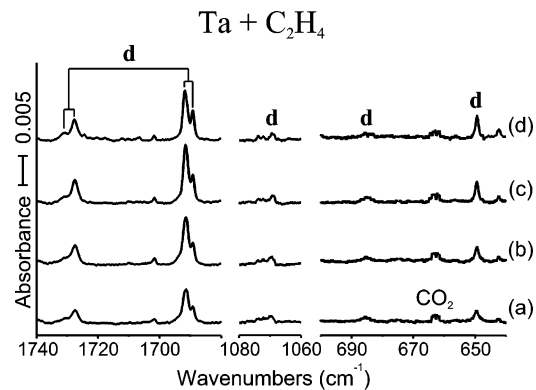
**Figure 4.** Energies of the plausible products in possible electronic states from reaction of Nb atoms with ethylene. Notice that the most stable product is the dihydrido complex ( $\text{NbH}_2\text{-C}_2\text{H}_2$ ) in its doublet ground state, which is identified in the infrared spectra (Figures 1–3).

a small amount of  $\text{MH}_2\text{-C}_2\text{D}_2$  and  $\text{MD}_2\text{-C}_2\text{H}_2$  along with  $\text{MHD-CHCD}$  also suggests that additional migration of hydrogen atoms occurs between the carbon and metal atoms in excited species formed initially during deposition, owing to the reaction energy.

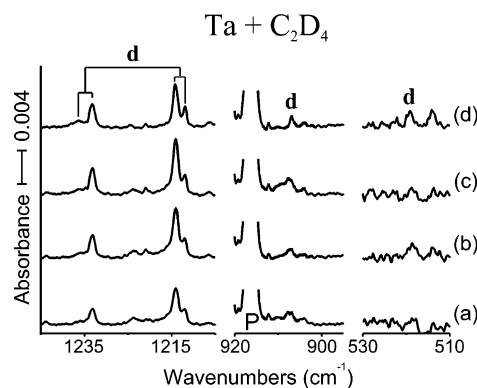
This is the first direct observation of the  $\text{NbH}_2\text{-C}_2\text{H}_2$  complex. Davis and co-workers<sup>6</sup> studied hydrogen abstraction reactions of ethylene by Nb atoms using crossed molecular beams ( $\text{Nb} + \text{C}_2\text{H}_4 \rightarrow \text{NbC}_2\text{H}_2 + \text{H}_2$ ) and observed the angular distribution of  $\text{NbC}_2\text{H}_2$  by electron impact and photoionization mass spectrometry. They suggested that the  $\pi$ -complex [ $\text{Nb}\cdots\text{C}_2\text{H}_4(^6\text{A}_1)$ ] is formed first but that the rest of the reaction occurs on the quartet potential surface and  $\text{NbH}_2\text{-C}_2\text{H}_2$  is the most stable reaction intermediate. They also claimed that there is no energy barrier between the insertion and dihydrido reaction intermediates, and accordingly, this product is expected to be formed directly in our matrix isolation experiment.

Figure 4 shows the energies of the plausible products from the reaction of Nb with ethylene calculated with B3LYP/6-311++G(3df,3pd)/SDD [the MP2 energy differences are 40–60% larger]. The strongly bound metallacyclopropane complex [ $\text{Nb-C}_2\text{H}_4(^4\text{B}_1)$ ] is slightly more stable than the  $\pi$ -complex [ $\text{Nb}\cdots\text{C}_2\text{H}_4(^6\text{A}_1)$ ]. The metallacyclopropane complex is believed to transform to the insertion product, which has a  $\text{C}_1$  structure in its quartet ground state. Clearly the dihydrido complex ( $\text{NbH}_2\text{-C}_2\text{H}_2$ ) in the doublet ground state is the most stable reaction product. However, on the quartet potential surface, we find that the dihydrido complex is less stable than the insertion complex, in contrast to the inference in Figure 2 of ref 6. Thus, the less stable quartet dihydrido complex can eliminate dihydrogen, but the more stable doublet dihydrido complex is trapped here in the solid matrix.

In this study  $\text{NbH}_2\text{-C}_2\text{H}_2$  in the  $^2\text{A}_2$  ground state is identified as the primary reaction product of  $\text{Nb} + \text{C}_2\text{H}_4$ . The metallacyclopropane complex [ $\text{Nb-C}_2\text{H}_4(^4\text{B}_1)$ ] is presumably formed and stable in the matrix, but the absorptions are expected to be too weak to observe unless the concentration is high. Unfortunately the absorptions of  $\text{Nb-C}_2\text{H}_2(^4\text{A}_2)$ , which is the remnant of hydrogen release, are also expected to be very weak. While the  $\text{NbH}_2$  fragment absorptions are quite strong in Figure 1, the  $\text{NbD}_2$  absorptions at 1154.1 and 1128.2  $\text{cm}^{-1}$  are much weaker in Figure 2, indicating that  $\text{D}_2$  elimination is relatively less efficient. The  $\text{NbHD}$  absorption at 1141.1  $\text{cm}^{-1}$  is also



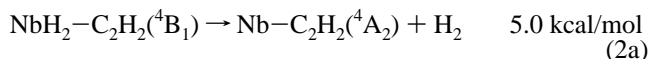
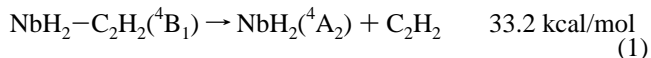
**Figure 5.** IR spectra in the regions 1740–1680, 1080–1060, and 700–640  $\text{cm}^{-1}$  for laser-ablated Ta atoms codeposited with  $\text{C}_2\text{H}_4$  in excess argon at 8 K and their variation: (a) Ta + 0.5%  $\text{C}_2\text{H}_4$  in Ar codeposited for 1 h; (b) after broad-band photolysis with  $\lambda > 420$  nm; (c) after annealing to 28 K; (d) after annealing to 36 K. **d** denotes the dihydrido product absorption.



**Figure 6.** IR spectra in the regions 1245–1205, 920–890, and 530–510  $\text{cm}^{-1}$  for laser-ablated Ta atoms codeposited with  $\text{C}_2\text{D}_4$  in excess argon at 8 K and their variation: (a) Ta + 0.5%  $\text{C}_2\text{D}_4$  in Ar codeposited for 1 h; (b) after broad-band photolysis with  $\lambda > 420$  nm; (c) after annealing to 20 K; (d) after annealing to 36 K. **d** denotes the dihydrido product absorption.

observed in Figure 2 because a small amount of  $\text{H}_2$  is present during reaction of  $\text{C}_2\text{D}_4$  due to cracking of diffusion pump oil.

$\text{NbH}_2$  can be produced directly from the dihydrido complex (eq 1), and it can also be formed in reaction of Nb atoms with the hydrogen molecules released from the dihydrido complex (eq 2). Clearly the reaction path in eq 2 is energetically much more favored than dissociation of the dihydrido complex into  $\text{NbH}_2$  and acetylene (eq 1).



The insertion product [ $\text{NbH-C}_2\text{H}_3(^4\text{A})$ ], which is 15 kcal/mol higher than the dihydrido complex [ $\text{NbH}_2\text{-C}_2\text{H}_2(^2\text{A}_2)$ ], is expected to show a strong Nb–H stretching absorption. The harmonic frequency of the hydrogen stretching mode is predicted at 1672.2  $\text{cm}^{-1}$  (Table S1, Supporting Information). A weak absorption marked **i** (for insertion product) is observed at 1595.8  $\text{cm}^{-1}$  ( $1595.8/1672.2 = 0.954$ ) among the water residue absorptions in the Nb +  $\text{C}_2\text{H}_4$  spectra, which increases upon photolysis ( $\lambda > 420$  nm), and a similar absorption with the same frequency also appears in the Nb +  $^{13}\text{C}_2\text{H}_4$  spectra (not shown).

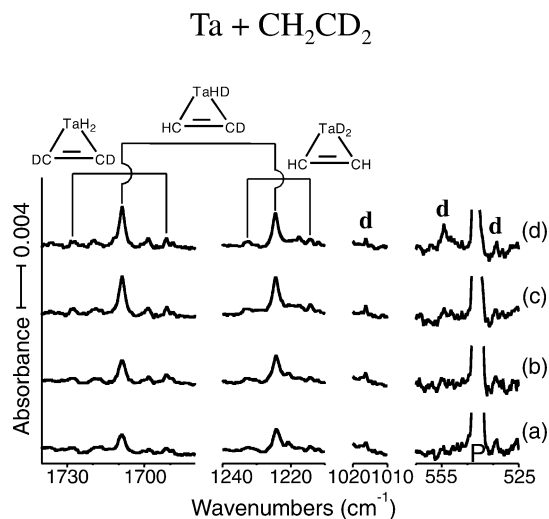


**Figure 7.** IR spectra in the regions 1740–1680, 1240–1210, 1020–1010, and 565–525  $\text{cm}^{-1}$  for laser-ablated Ta atoms codeposited with  $\text{CH}_2\text{CD}_2$  in excess argon at 8 K and their variation: (a) Ta + 0.5%  $\text{CH}_2\text{CD}_2$  in Ar codeposited for 1 h; (b) after broad-band photolysis with  $\lambda > 420$  nm; (c) after annealing at 28 K; (d) after annealing to 36 K. **d** denotes the dihydrido product absorption.

However, the corresponding absorptions are not observed in the  $\text{C}_2\text{D}_4$  and  $\text{CH}_2\text{CD}_2$  spectra, possibly because of the low absorption intensity. We tentatively assign the absorption at  $1595.8 \text{ cm}^{-1}$  to the Nb–H stretching mode of the insertion complex as listed in Table 1.

**Ta +  $\text{C}_2\text{H}_4$ .** Infrared spectra from the Ta +  $\text{C}_2\text{H}_4$  reaction are similar to the Nb +  $\text{C}_2\text{H}_4$  spectra. Figure 5 shows the Ta +  $\text{C}_2\text{H}_4$  spectra, and Figure 6 illustrates the corresponding Ta +  $\text{C}_2\text{D}_4$  spectra. Again the observed absorptions are all marked **d**. They increase about 50% upon photolysis ( $\lambda > 420$  nm) and increase another 30% in the early stage of annealing, in contrast to Nb. Similar variations in intensity on photolysis and annealing occur in the Ta +  $\text{CH}_2\text{CD}_2$  spectra (Figure 7), where triplet patterns are again observed.

The strongest absorptions are observed in the Ta–H stretching region at  $1727.5$  and  $1691.5 \text{ cm}^{-1}$  in Figure 5 with about 1:2 intensity ratio, which can be compared with  $\text{TaH}_2$  absorptions at  $1758.9$  and  $1733.9 \text{ cm}^{-1}$  examined in previous work.<sup>29</sup> No absorptions from binary tantalum hydrides are observed in this

study, unlike the Nb case. The two strong absorptions show essentially no  $^{13}\text{C}$  shifts, but deuteration leads to isotopic shifts of  $-494.4$  and  $-477.5 \text{ cm}^{-1}$  (H/D ratios of 1.401 and 1.393), respectively. The hydrogen stretching absorptions with 1:2 intensity ratio suggest that the major reaction product of the Ta +  $\text{C}_2\text{H}_4$  reaction has two Ta–H bonds, in line with the Nb case, and the energetically most favorable is  $\text{TaH}_2\text{--C}_2\text{H}_4$ . The triplet patterns at  $1727.9$ ,  $1708.8$ , and  $1691.4 \text{ cm}^{-1}$  and at  $1232.9$ ,  $1224.4$ , and  $1214.3 \text{ cm}^{-1}$  with  $\text{CH}_2\text{CD}_2$  again verify that the product contains two Ta–H bonds. The other product absorptions all relate to the predicted vibrational characteristics for  $\text{TaH}_2\text{--C}_2\text{H}_2$  as expected<sup>30,31</sup> and as shown by comparison of observed and calculated frequencies (Table 3). Again the calculated anharmonic frequencies are closer to the observed values than the calculated harmonic frequencies.

The absorption at  $1404 \text{ cm}^{-1}$  (not illustrated) in the Ta +  $\text{C}_2\text{H}_4$  spectra shows a  $^{13}\text{C}$  shift of  $-53.9 \text{ cm}^{-1}$  ( $^{12}\text{C}/^{13}\text{C}$  ratio of 1.040). On the basis of the frequency and substantial  $^{13}\text{C}$  shift, the band is assigned to the C=C stretching mode of the dihydrido complex without observation of the deuterium counterpart. The absorption at  $1069.5 \text{ cm}^{-1}$  has its D and  $^{13}\text{C}$  counterparts at  $-907.7$  and  $-1054.1 \text{ cm}^{-1}$  (H/D and  $^{12}\text{C}/^{13}\text{C}$  ratios of 1.178 and 1.015), and it is designated to the HCCH in-plane bending mode on the basis of the frequency and the considerable D shift. The weak absorption at  $685.6 \text{ cm}^{-1}$  is assigned to the  $\text{TaH}_2$  scissoring mode without the D and  $^{13}\text{C}$  counterparts. The relatively strong product absorption at  $649.4 \text{ cm}^{-1}$  shows a small  $^{13}\text{C}$  shift of  $-6.1 \text{ cm}^{-1}$  and is attributed to the HCCH out-of-plane bending mode. In the further low-frequency region, the band at  $519 \text{ cm}^{-1}$  in Figure 6 probably arises from the Ta–C<sub>2</sub> stretching mode.

The predicted energies for the plausible reaction products of Ta +  $\text{C}_2\text{H}_4$  are shown in Figure 8. The metallacyclopropane complex  $[\text{Ta--C}_2\text{H}_4(^4\text{B}_1)]$  is considerably more stable (25 kcal/mol) than the  $\pi$ -complex  $[\text{Ta}\cdots\text{C}_2\text{H}_4(^6\text{A}_1)]$ . The insertion complex  $[\text{TaH--C}_2\text{H}_3(^4\text{A}'')]$  is energetically comparable with the metallacyclopropane complex, but the dihydrido complex  $[\text{TaH}_2\text{--C}_2\text{H}_2(^2\text{A})]$  is clearly the most stable among the plausible products. Parallel to the Nb case, hydrogen release from the dihydrido complex is more favored than dissociation into  $\text{TaH}_2\text{--}(^4\text{A}_2)$  and  $\text{C}_2\text{H}_2$  in the quartet state (eqs 3 and 4). Although the insertion complex is not observed for tantalum, it is an intermediate in the formation of the dihydrido complex, and its frequencies are given in Table S2 (Supporting Information).

**TABLE 3: Observed and Calculated Frequencies of the Fundamental Bands of  $\text{TaH}_2\text{--C}_2\text{H}_2$  in the Ground  $^2\text{A}$  State<sup>a</sup>**

description	$\text{TaH}_2\text{--C}_2\text{H}_2$				$\text{TaD}_2\text{--C}_2\text{D}_2$			$\text{TaH}_2\text{--}^{13}\text{C}_2\text{H}_2$			$\text{TaHD--C}_2\text{HD}$		
	obs	anharm <sup>b</sup>	harm.	int	obs	harm.	int	obs	harm.	int	obs	harm.	int
CH sym str		3048.2	3198.6	2		2388.8	0		3177.1	2		3172.9	2
CH asym str		3026.5	3163.2	3		2316.9	1		3153.6	3		2361.7	1
$\text{TaH}_2$ sym str	1727.5	1727.7	1775.5	217	1233.1	1258.2	114	1727.5	1775.5	217	1708.7	1768.3	253
$\text{TaH}_2$ asym str	1691.5	1690.9	1740.8	438	1214.0	1237.1	222	1691.5	1740.8	438	1224.5	1240.7	206
C=C str	1404.4	1417.6	1456.5	14		1397.6	7	1350.5	1403.4	13		1426.1	11
HCCH IP asym bend	1069.5	1066.4	1092.3	54	907.7	940.2	21	1054.1	1073.3	55	1014.3	1037.2	39
HCCH OOP asym bend		927.3	951.3	3		761.0	3		941.5	3		877.2	11
HCCH IP sym bend		815.1	836.0	3		617.5	9		834.9	3		720.0	8
$\text{TaH}_2$ scis	685.6	691.4	744.0	64		573.6	32		740.9	62		680.5	45
HCCH OOP sym bend	649.4	669.1	671.2	58		502.8	26	634.3	666.7	59	554.1	584.4	34
$\text{TaC}_2$ asym str		613.5	622.6	43	519.0	544.7	33		608.9	39	533.9	554.3	19
$\text{TaC}_2$ sym str		525.4	545.1	6		468.4	11		528.8	6		524.6	20
$\text{TaH}_2$ twist		399.8	432.8	14		325.7	7		429.7	15		348.9	7
$\text{TaH}_2$ rock		321.0	377.8	7		274.8	4		376.9	7		295.4	4
$\text{TaH}_2$ wag		52.8	216.0	74		155.3	38		215.7	74		197.8	64

<sup>a</sup> Frequencies are given in reciprocal centimeters, and calculated intensities are in kilometers per mole. Calculations were done with B3LYP/6-311++G(3df,3pd), and SDD core potential and basis set were used for Ta. Unlike  $\text{VH}_2\text{--C}_2\text{H}_2$  and  $\text{NbH}_2\text{--C}_2\text{H}_2$ ,  $\text{TaH}_2\text{--C}_2\text{H}_2$  has a  $\text{C}_1$  structure in its doublet ground state. <sup>b</sup> Calculated anharmonic frequencies.

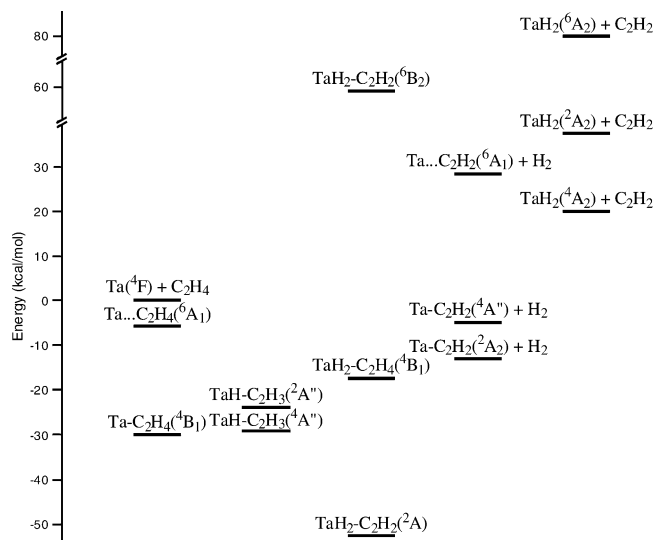
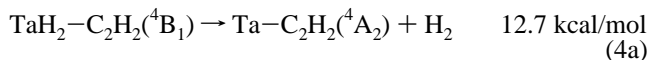
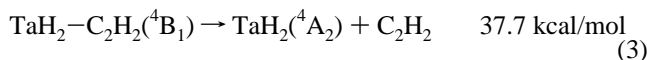


**Figure 8.** Energies of the plausible products in possible electronic states from reaction of Ta atoms with ethylene. Notice that the most stable product ( $\text{TaH}_2\text{-C}_2\text{H}_2$ ) in its doublet ground state is about 30 kJ/mol more stable than the metallocyclic product [ $\text{Ta-C}_2\text{H}_4(^4\text{B}_1)$ ] and the insertion complex [ $\text{TaH-C}_2\text{H}_3(^4\text{A}'')$ ]. Only the dihydrido complex is identified in the infrared spectra (Figures 5–7).



**V + C<sub>2</sub>H<sub>4</sub>.** The V + C<sub>2</sub>H<sub>4</sub> spectra shown in Figure 9 are much more congested than the corresponding Nb and Ta spectra. The product absorptions are marked **d** or **i** for the two product absorption groups, and the measured frequencies are compared with calculated frequencies in Tables 4 and 5. The **d** absorptions are weaker relative to the Nb and Ta cases and as a result, a smaller number of them are observed. The **d** absorptions almost triple upon photolysis ( $\lambda > 320$  nm) but slightly decrease upon the following photolysis with longer wavelength ( $\lambda > 420$  nm). The **d** absorptions at 1661.5 and 1638.5  $\text{cm}^{-1}$  with about 1:2 intensity ratio show D shifts of  $-463.7$  and  $-447.2$   $\text{cm}^{-1}$  (Figure 10) and H/D ratios of 1.387 and 1.375, and the spectra reveal essentially no <sup>13</sup>C shifts. These bands are in excellent agreement with the two modes calculated for  $\text{VH}_2\text{-C}_2\text{H}_2$  (1.0% and 0.7% below calculated, Table 4), and they exhibit a 23.0  $\text{cm}^{-1}$  mode separation, which is near the 28.2  $\text{cm}^{-1}$  calculated mode separation. This stable product increases during our irradiation sequence. We therefore disagree with the tentative assignments of 1644 and 1552  $\text{cm}^{-1}$  bands to this molecule made by Thompson and Parnis.<sup>3b</sup> These bands do not fit the B3LYP frequency calculations nearly as well as our above bands, and the mode separation is too high for both stretching modes of a  $\text{VH}_2$  subgroup, on the basis of our DFT calculations. The earlier workers used a much higher reagent concentration (1.4%) and their product could involve more than one ethylene molecule.

In the same frequency region, the V–H stretching absorptions of binary vanadium hydrides are observed (e.g., 1532.4 and 1508.3  $\text{cm}^{-1}$  for  $\text{VH}_2$  and 1123.6 and 1092.0  $\text{cm}^{-1}$  for  $\text{VD}_2$ ), and the V–H stretching frequencies of binary vanadium hydrides increase with the valence of vanadium.<sup>29</sup> In addition, the experiment with  $\text{CH}_2\text{CD}_2$  gave triplet absorptions for the diagnostic **d** absorptions at 1658.7, 1649.1, and 1638.6  $\text{cm}^{-1}$

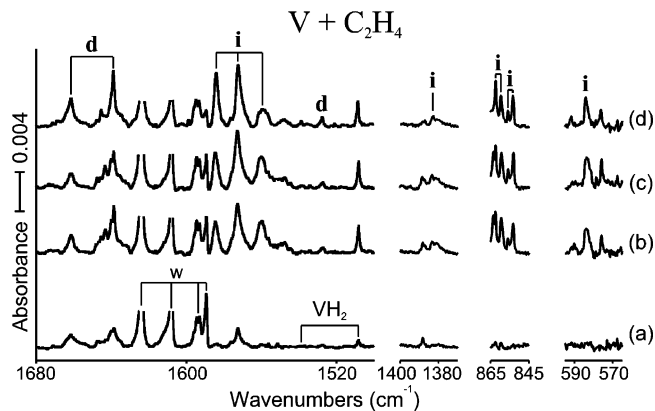


**Figure 9.** IR spectra in the regions 1680–1500, 1400–1370, 865–845, and 595–565  $\text{cm}^{-1}$  for laser-ablated V atoms codeposited with C<sub>2</sub>H<sub>4</sub> in excess argon at 8 K and their variation: (a) V + 0.5% C<sub>2</sub>H<sub>4</sub> in Ar codeposited for 1 h; (b) after broad-band photolysis with  $\lambda > 320$  nm; (c) after broad-band photolysis with  $\lambda > 420$  nm; (d) after annealing to 36 K. **d** and **i** denote the product absorption groups. The vanadium spectra are more congested than the niobium and tantalum spectra, and two primary products [dihydrido (**d**) and insertion (**i**) complexes] are identified in the infrared spectra, unlike the niobium and tantalum cases.

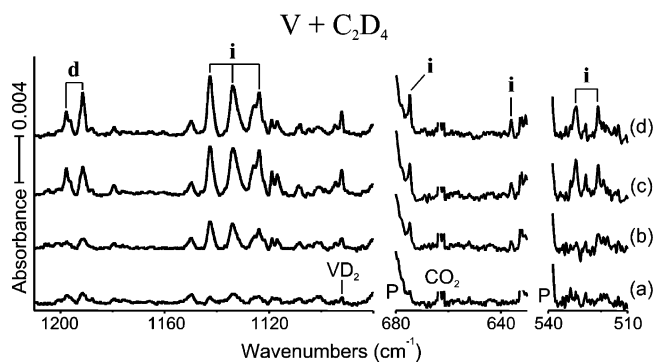


**Figure 10.** IR spectra in the regions 1210–1080, 680–630, and 540–510  $\text{cm}^{-1}$  for laser-ablated V atoms codeposited with C<sub>2</sub>D<sub>4</sub> in excess argon at 8 K and their variation: (a) V + 0.5% C<sub>2</sub>D<sub>4</sub> in Ar codeposited for 100 min; (b) after broad-band photolysis with  $\lambda > 420$  nm; (c) after broad-band photolysis with  $\lambda > 320$  nm; (d) after annealing to 20 K. **d** and **i** denote the dihydrido and insertion product absorption groups.

and at 1199.3, 1193.1, and 1190.1  $\text{cm}^{-1}$  (see Figure S1). These V–H stretching absorptions indicate that the dihydrido product ( $\text{VH}_2\text{-C}_2\text{H}_2$ ) is also formed in reaction of V with C<sub>2</sub>H<sub>4</sub>. Another **d** absorption at 1527.8  $\text{cm}^{-1}$  has its <sup>13</sup>C counterpart at 1478.3  $\text{cm}^{-1}$  (<sup>12</sup>C/<sup>13</sup>C frequency ratio = 1.033), and it is attributed to the C=C stretching mode without observation of the D counterpart.

In contrast to the Nb and Ta cases, a large group of absorptions marked **i** is observed in the V + C<sub>2</sub>H<sub>4</sub> spectra. In Figure 9, these bands increase dramatically upon the first photolysis ( $\lambda > 320$  nm) and increase slightly upon the following photolysis ( $\lambda > 420$  nm) and upon annealing. Note that the major bands (1584.6, 1572.8, and 1560.1  $\text{cm}^{-1}$ ) are split by the matrix. In the C<sub>2</sub>D<sub>4</sub> spectra in Figure 10, upon the first photolysis with longer wavelength ( $\lambda > 420$  nm) they increase about 300%, and on the following photolysis with shorter wavelength ( $\lambda > 320$  nm) they increase another 300%, and the major bands are also split by the matrix (1142.5, 1133.9, and 1123.8  $\text{cm}^{-1}$ ). The overall increase in intensity of the deuterated products resulting from C–D insertion on photolysis is often much higher than hydrogen counterparts.<sup>31</sup> The strongest

**TABLE 4: Observed and Calculated Frequencies of the Fundamental Bands of  $\text{VH}_2\text{-C}_2\text{H}_2$  in the Ground  $^2\text{A}_2$  State<sup>a</sup>**

mode description <sup>b</sup>	$\text{VH}_2\text{-C}_2\text{H}_2$				$\text{VD}_2\text{-C}_2\text{D}_2$			$\text{VH}_2\text{-}^{13}\text{C}_2\text{H}_2$			$\text{VHD-C}_2\text{HD}$		
	obs	anharm <sup>c</sup>	harm.	int	obs	harm.	int	obs	harm.	int	obs	harm.	int
A <sub>1</sub> CH str		3088.5	3227.0	2		2438.4	6		3213.0	1		3209.9	1
A <sub>1</sub> $\text{VH}_2$ sym str	1661.5	1678.7	1741.7	323	1197.8	1236.2	187	1661.5	1741.2	330	1649.1	1727.2	395
A <sub>1</sub> C=C str	1527.8	1540.4	1569.9	42		1488.9	12	1487.3	1514.3	35		1528.2	26
A <sub>1</sub> HCCH IP bend		747.5	770.2	25		551.1	7		770.0	26		666.9	8
A <sub>1</sub> $\text{VH}_2$ scis		692.3	732.5	71		633.1	31		728.0	71		681.2	64
A <sub>1</sub> $\text{VC}_2$ sym str		527.2	543.4	4		443.5	17		532.3	3		504.8	43
A <sub>2</sub> HCCH OOP bend		859.4	874.8	0		708.9	0		864.5	0		819.3	10
A <sub>2</sub> $\text{VH}_2$ twist		356.5	386.8	0		289.0	0		384.3	0		379.4	62
B <sub>1</sub> $\text{VH}_2$ str	1638.5	1650.5	1713.6	474	1191.4	1233.0	247	1638.5	1713.7	474	1193.1	1235.6	223
B <sub>1</sub> HCCH OOP bend		655.4	664.8	64		503.5	34		661.3	64		558.0	38
B <sub>1</sub> $\text{VH}_2$ rock		336.2	335.3	0		247.0	0		334.7	0		275.5	1
B <sub>2</sub> CH str		3048.4	3191.6	0		2345.1	0		3182.2	0		2392.7	3
B <sub>2</sub> HCCH IP bend		965.8	997.9	69		875.5	26		978.5	70	912.1	952.8	50
B <sub>2</sub> $\text{VC}_2$ str		569.1	585.3	87		494.7	67		573.5	85		526.0	42
B <sub>2</sub> $\text{VH}_2$ wag		355.4	384.5	150		279.9	78		383.9	148		289.2	44

<sup>a</sup> Frequencies are given in reciprocal centimeters, and harmonic calculated intensities are in kilometers per mole. Calculations were done with B3LYP/6-311++G(3df,3pd), and an all-electron basis set was used for V. <sup>b</sup> Mode descriptions and symmetries are for  $\text{C}_{2v}$  structure in doublet ground state. <sup>c</sup> Calculated anharmonic frequencies.

**TABLE 5: Observed and Calculated Frequencies of the Fundamental Bands of  $\text{VH-CHCH}_2$  ( $^4\text{A}$ ) in the Most Stable  $\text{C}_1$  Structure<sup>a</sup>**

description	$\text{VH-CHCH}_2$				$\text{VD-CDCl}_2$			$\text{VH-}^{13}\text{CH}^{13}\text{CH}_2$			$\text{VH-CHDCD}$			$\text{VD-CDHCH}$		
	obs	anharm <sup>b</sup>	harm.	int	obs	harm.	int	obs	harm.	int	obs	harm.	int	obs	harm.	int
$\text{C}_2\text{-H}_3$ str		3025.5	3165.1	8		2350.2	1		3154.3	8		2349.3	0		3164.9	7
$\text{C}_1\text{-H}_2$ str		2967.1	3120.5	9		2299.2	3		3111.0	9		2295.5	4		3120.1	9
$\text{C}_1\text{-H}_1$ str	2569.0	2563.8	2795.0	34	1989.8	2044.0	18	2561.9	2788.3	34		2795.6	35		2048.1	17
C-C str		1575.8	1630.6	21		1478.3	4		1610	151		1560.4	14		1526.8	3
V-H str	1572.8	1574.2	1601.4	425	1133.9	1144.8	236	1572.9	1598.7	297	1572.9	1603.6	430	1143.1	1153.6	113
$\text{CH}_2$ scis	1383.2	1383.7	1424.4	29	1092.0	1099.6	15		1387.9	24		1366.1	29		1286.3	28
HCCH IP sym bend		1178.5	1207.2	21		1000.0	9		1189.5	22		1007.4	11		1139.4	
HCCH OOP bend		988.1	1009.7	12		767.1	0		1005.3	13		763.8	1		986.6	1
$\text{CH}_2$ wag	862.	878.0	898.6	42	674.7	704.3	31	858.2	889.1	14		851.6	33		802.2	50
HCCH IP asym bend	853.3	871.4	880.4	38	636.0	643.2	18	852.1	877.7	38		656.1	16		828.6	39
C-V str	583.9	573.0	585.3	67	529.5	529.7	46	571.2	572.7	68		547.2	87	554.6	564.2	37
CVH bend		407.8	429.0	63		330.0	26		426.3	62		407.8	69		352.0	21
$\text{CH}_2$ twist		330.6	330.8	28		266.4	17		328.7	29		288.2	18		288.5	12
CCV bend		236.6	275.5	88		219.5	58		270.9	84		258.0	78		233.7	71
VH OOP bend		93.8	118.5	133		87.1	67		118.1	133		117.0	132		88.2	67

<sup>a</sup> Frequencies are given in reciprocal centimeters, and harmonic intensities are in kilometers per mole. Calculations were done with B3LYP/6-311++G(3df,3pd), and an all-electron basis was used for V. Intensities are all calculated values.  $\text{C}_2\text{H}_3\text{-VH}$  has the most stable  $\text{C}_1$  structure in its quartet ground state, where the hydrogen atom bonded to the metal atom is above the nearly planar structure formed by the other atoms (see Figure 12). <sup>b</sup> Calculated anharmonic frequencies.

**i** band at  $1572.8\text{ cm}^{-1}$  shows a D shift of  $-438.9\text{ cm}^{-1}$  (H/D ratio 1.387) and almost no  $^{13}\text{C}$  shift.

The group of V-H stretching bands with frequencies lower than those of  $\text{VH}_2\text{-C}_2\text{H}_2$  and more comparable to  $\text{VH}_2$  frequencies suggest that another primary product, with a lower valence of vanadium, is formed in the reaction of V with  $\text{C}_2\text{H}_4$ . The energies of the plausible reaction products of V +  $\text{C}_2\text{H}_4$  are shown in Figure 11. The most stable reaction product is  $\text{VH-C}_2\text{H}_3$  in its quartet ground state, in contrast to the fact that the dihydrido complex in the doublet ground state is the most stable in the Nb and Ta system. It is also notable that the dihydrido complex becomes more stable relative to the insertion product with going down the family group.

The other **i** absorptions also support formation of the insertion complex,  $\text{VH-C}_2\text{H}_3$ . The absorption at  $1383.2\text{ cm}^{-1}$  has its D counterpart at  $1092.0\text{ cm}^{-1}$  (H/D ratio = 1.267) and is assigned to the  $\text{CH}_2$  scissoring mode. The absorption at  $862.5\text{ cm}^{-1}$  shows D and  $^{13}\text{C}$  shifts of  $-187.8$  and  $-4.3\text{ cm}^{-1}$  (H/D and  $^{12}\text{C}/^{13}\text{C}$  ratios of 1.278 and 1.005) and is attributed to the  $\text{CH}_2$  wagging mode on the basis of the frequency and magnitudes of isotopic shift. Another absorption at  $853.3\text{ cm}^{-1}$  shows D and  $^{13}\text{C}$  shifts

of  $-217.3$  and  $-1.2\text{ cm}^{-1}$  (H/D and  $^{12}\text{C}/^{13}\text{C}$  ratios of 1.342 and 1.001) and is attributed to the HCCH asymmetric in-plane bending mode. The band at  $583.9\text{ cm}^{-1}$  has its D and  $^{13}\text{C}$  counterparts at  $529.5$  and  $571.2\text{ cm}^{-1}$  (H/D and  $^{12}\text{C}/^{13}\text{C}$  ratios of 1.103 and 1.022) and is assigned to the C-V stretching mode. In the high-frequency region, the weak absorption at  $2569.0\text{ cm}^{-1}$  has its deuterium and  $^{13}\text{C}$  counterparts at  $1989.8$  and  $2561.9\text{ cm}^{-1}$  (not shown), which are assigned to the C-H stretching mode. Although this absorption is low for a typical C-H stretching frequency, our B3LYP calculation predicts this mode to be considerably anharmonic, as the calculated anharmonic value ( $2563.8\text{ cm}^{-1}$ ) is much lower than the calculated harmonic value ( $2795.0\text{ cm}^{-1}$ ) as given in Table 5.

The observed **d** and **i** frequencies are in good agreement with the calculated frequencies, within the limits of the approximations involved,<sup>30,31</sup> for  $\text{VH}_2\text{-C}_2\text{H}_2(^2\text{A}_2)$  and  $\text{VH-C}_2\text{H}_3(^4\text{A})$  as shown in Tables 4 and 5. The most stable structure for the insertion product in its quartet ground state is a  $\text{C}_1$  structure as shown in Figure 12, where the hydrogen atom bonded to the V atom is above the nearly planar structure formed by the other six atoms, and its frequencies are listed in Table 5. However,

**TABLE 6: Calculated Frequencies of the Fundamental Bands of Planar VH-CHCH<sub>2</sub> (<sup>4</sup>A')<sup>a</sup>**

description	VH-CHCH <sub>2</sub>			VD-CDCH <sub>2</sub>		VH- <sup>13</sup> CH <sup>13</sup> CH <sub>2</sub>		VH-CDCHD		VD-CHCHD	
	anharm <sup>b</sup>	harm.	int	harm.	int	harm.	int	harm.	int	harm.	int
A' C <sub>2</sub> -H <sub>3</sub> str	2998.9	3148.1	14	2336.0	3	3137.5	15	3147.9	13	2334.7	2
A' C <sub>1</sub> -H <sub>2</sub> str	2966.1	3108.0	14	2289.7	4	3098.6	15	3107.2	14	2283.1	5
A' C <sub>1</sub> -H <sub>1</sub> str	2706.7	2873.3	34	2102.2	18	2866.2	35	2108.7	18	2875.1	37
A' C-C str	1552.2	1610.0	180	1491.5	7	1568.7	36	1536.0	5	1539.0	16
A' V-H str	1541.7	1594.7	236	1144.7	220	1604.3	380	1152.2	105	1603.4	400
A' CH <sub>2</sub> scis	1393.2	1413.2	27	1067.3	15	1384.8	25	1290.5	31	1334.3	23
A' HCCH IP asym bend	1195.2	1216.5	20	1003.5	5	1199.3	21	1139.2	123	1014.8	10
A' HCCH IP sym bend	898.7	898.0	32	657.7	16	894.7	32	831.7	30	672.5	18
A' C <sub>2</sub> -V str	547.1	551.1	87	501.4	55	539.9	89	530.5	48	522.0	107
A' CVH bend	412.3	408.4	70	305.9	37	406.4	67	308.7	40	400.9	53
A' CCV bend	91.0	140.9	39	123.2	31	138.0	37	129.0	33	133.4	36
A'' HCCH OOP bend	1006.2	1022.0	12	769.3	1	1018.2	12	992.8	1	767.1	0
A'' CH <sub>2</sub> wag	900.6	912.9	30	721.3	24	902.6	29	806.8	43	881.6	26
A'' CH <sub>2</sub> twist	347.9	361.4	1	271.0	2	359.3	1	320.2	6	302.3	2
A'' VH OOP bend	110.5	194.6	140	142.7	73	194.3	140	144.4	72	188.5	134

<sup>a</sup> Frequencies are given in reciprocal centimeters, and harmonic intensities are in kilometers per mole. Calculations were done with B3LYP/6-311++G(3df,3pd), and an all-electron basis was used for V. Intensities are all calculated values. C<sub>2</sub>H<sub>3</sub>-VH has a local energy minimum with a planar structure in its quartet ground state. <sup>b</sup> Calculated anharmonic frequencies.

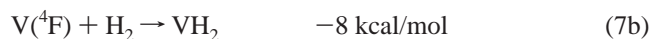
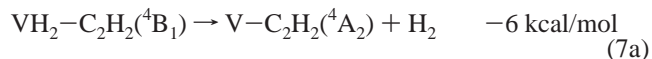
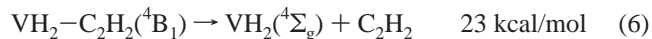
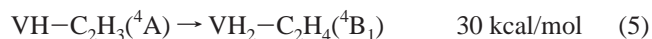
further examination leads to another stable structure for the insertion product, which is planar and only 3.2 kcal/mol higher in energy (<sup>4</sup>A'). The energy difference is too small to determine with confidence which structure is more stable in the matrix. The predicted frequencies for the planar structure are also listed in Table 6, many of which are close to those for the C<sub>1</sub> structure.

Many *i* absorptions including the V-H stretching absorptions in fact appear as pairs as shown in Figure 9. It is also noticeable that the intensity ratios of the pairs, including that of the two strong V-H stretching absorptions at 1584.6 and 1572.8 cm<sup>-1</sup>, vary in the process of photolysis and annealing. It is, however, difficult to distinguish one absorption from the other. For example, the predicted difference in the V-H stretching frequencies for the two insertion product structures is only 7 cm<sup>-1</sup>. No attempt is made to distinguish the structures in assigning the absorptions.

The observed product absorptions in the Ta + C<sub>2</sub>H<sub>4</sub> spectra are all attributed to the dihydrido complex, and similarly most product absorptions in Nb + C<sub>2</sub>H<sub>4</sub> spectra arise from the dihydrido product and only a weak absorption is tentatively assigned to the Nb-H stretching mode of the insertion product. However, in the V + C<sub>2</sub>H<sub>4</sub> spectra, more absorptions from the insertion product (VH-C<sub>2</sub>H<sub>3</sub>) are observed than those from the dihydrido complex, and this trend is consistent with the relative energies of the two major products in their ground states as shown in Figures 4, 8, and 11. A similar trend is observed among the methane activation products by early transition metals in recent studies.<sup>31</sup> The methylidene and methylidyne products (CH<sub>2</sub>=MH<sub>2</sub> and CH≡MH<sub>3</sub>) are more favored than the insertion product (CH<sub>3</sub>-MH) by the heavier metals.

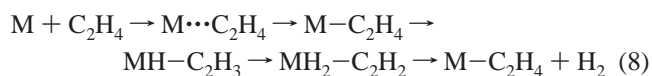
The binary VH<sub>2</sub> absorptions are observed at 1532.4 and 1508.3 cm<sup>-1</sup> in Figure 9, which increase dramatically along with the *d* and *i* absorptions upon photolysis (λ > 320 nm). It is notable that the NbH<sub>2</sub> stretching absorptions in Figures 1 and 2 remain almost unchanged upon photolysis, and no hydrogen stretching absorptions are observed in the Ta spectra. The hydrogen elimination reaction of ethylene by Ta is apparently less effective than for Nb, while vanadium can undergo the reaction even upon photolysis, generating VH<sub>2</sub>. The dihydrido complex, which is considered as the reaction intermediate prior to detachment of hydrogen,<sup>6,12</sup> is formed predominantly in the reaction of Ta + C<sub>2</sub>H<sub>4</sub>, but hydrogen elimination hardly occurs. Note that the Ta dihydrido complex is very stable relative to other plausible products as shown in Figure 8.

In the vanadium system, the rearrangement from VH-C<sub>2</sub>H<sub>3</sub> (<sup>4</sup>A) to VH<sub>2</sub>-C<sub>2</sub>H<sub>4</sub> (<sup>4</sup>B<sub>1</sub>) requires 30 kcal/mol on the quartet potential surface (eq 5), which is compared with 15 and 12 kcal/mol in the Nb and Ta systems, respectively. Photolysis, on the other hand, leads vanadium atoms isolated in the matrix to react with nearby ethylene molecules, and once the dihydrido complex in the quartet state is formed, hydrogen release easily follows (eq 7a). The eliminated hydrogen can in turn react with another vanadium atom to form VH<sub>2</sub> (eq 7b).



Throughout this study, weak absorptions for VO, NbO, and TaO molecules<sup>20a</sup> are also observed at 983.2, 970.6, and 1014.2 cm<sup>-1</sup>, but they are too weak to give observable reaction products. The metal dioxide absorptions, through antisymmetric stretching modes, are stronger.

**Reaction Mechanisms.** Previous studies on hydrogen elimination dynamics from ethylene using neutral early transition-metal atom reactions have proposed the following reaction pathway (eq 8):<sup>4,6,12,13</sup>



While the π-complex (M⋯C<sub>2</sub>H<sub>4</sub>) has the sextet ground state in case of Nb, the rest of the reaction is believed to occur on the quartet potential surface.<sup>6</sup> Our experiments with CH<sub>2</sub>CD<sub>2</sub> demonstrate clearly that the dihydrido complex is formed in most part by β-hydrogen transfer in the insertion complex since all three possible mixed H/D isotopic complexes are formed (see Figures 3 and 7). Note from the insertion complex structures (Figure 12) that a β-hydrogen is substantially closer to the metal center than the remaining α-hydrogen, so β-hydrogen transfer on visible light excitation of the insertion complex is a straightforward process. There is in addition some further exchange of H and D atoms in excited species formed in the initial exothermic reaction.

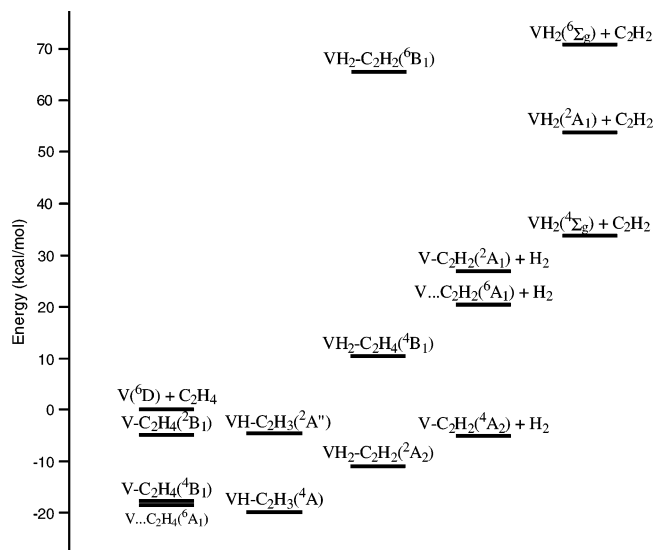
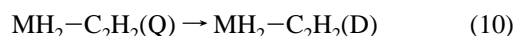
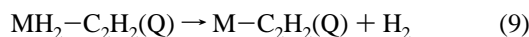


**Figure 11.** Energies of the plausible products in possible electronic states from reaction of V atoms with ethylene. Notice that the most stable product is the insertion complex (VH–C<sub>2</sub>H<sub>3</sub>) in its ground quartet state, which is comparable in energy with V–C<sub>2</sub>H<sub>4</sub>(<sup>4</sup>B<sub>1</sub>) and V...C<sub>2</sub>H<sub>4</sub>-(<sup>6</sup>A<sub>1</sub>) but 9 kJ/mol more stable than VH<sub>2</sub>–C<sub>2</sub>H<sub>2</sub>(<sup>2</sup>A<sub>2</sub>). Both dihydrido and insertion complexes are identified in the infrared spectra (Figures 9 and 10).

If the hydrogen elimination occurs on the quartet potential surface, as the previous reaction dynamics studies presume,<sup>6</sup> the difference in energy between the dihydrido complex and MC<sub>2</sub>H<sub>2</sub> + H<sub>2</sub> is probably an important factor. The differences in energy are –6, 5, and 13 kcal/mol for V, Nb, and Ta as shown above, respectively, indicating that hydrogen release from the dihydrido complex becomes more difficult with going down the column. The hydrogen release from the dihydrido complex in the doublet ground state is far more difficult; however, a similar tendency for hydrogen release from the dihydrido complex is also found in the doublet potential surface. The reaction energies are 23, 33, and 38 kcal/mol for V, Nb, and Ta, respectively.

The present results in fact support the presumption that the hydrogen elimination reaction occurs on the quartet potential surface. The relative yields of the primary products and the metal dihydrides are consistent with their relative energies on the quartet potential surface. Hydrogen release from the dihydrido complex in the quartet state is expected to be relatively slow due to a potential energy barrier (eq 9).<sup>6,12</sup> If a level crossing to the doublet state occurs instead of hydrogen elimination, the dihydrido complex relaxes into the stable doublet ground state (eq 10). The present results indicate that the competition between the two reactions mostly likely determines the relative yield of the metal dihydride and the dihydrido complex products.



**Structure.** The predicted structures for the identified reaction products are shown in Figure 12. Our BPW91 and MP2 calculations also give similar structures (Figure S2). The NbH<sub>2</sub>–C<sub>2</sub>H<sub>2</sub> and VH<sub>2</sub>–C<sub>2</sub>H<sub>2</sub> complexes have C<sub>2v</sub> structures, which are consistent with the structures of the dihydrido complexes of early transition metals predicted in the earlier studies.<sup>6,12</sup> On the other hand, TaH<sub>2</sub>–C<sub>2</sub>H<sub>2</sub> has a C<sub>1</sub> structure, where the two Ta–H bonds are not equivalent. Simon et al.<sup>11</sup> theoretically investigated possible configurations of the Ta–C<sub>2</sub>H<sub>4</sub><sup>+</sup> ion,

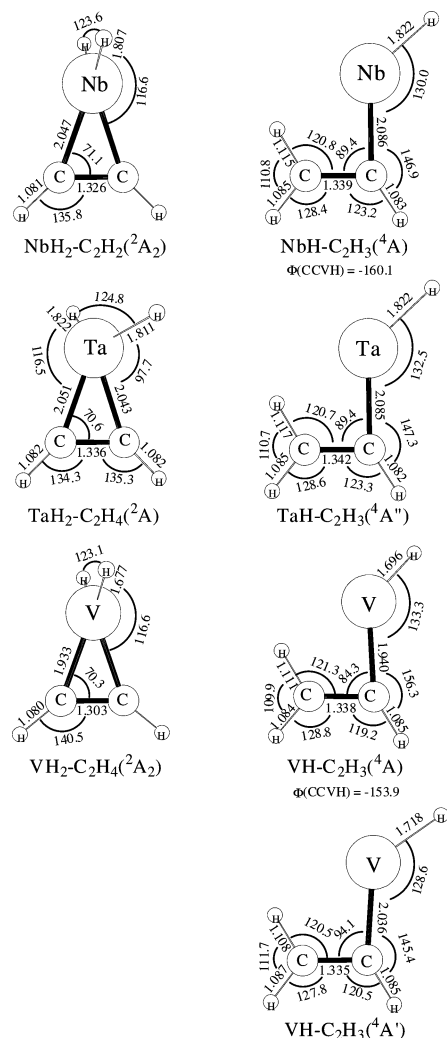


**Figure 12.** Optimized molecular structures of the dihydrido complexes of group 5 metals and the V insertion complex in the ground electronic states. The Nb and V dihydrido complexes have C<sub>2v</sub> structures, but the Ta complex has a C<sub>1</sub> structure. Calculations show that there are at least two stable configurations with comparable energies for the V insertion complex. The C<sub>1</sub> structure is 3.2 kJ/mol lower than the C<sub>s</sub> structure. Computations were carried out with B3LYP and the 6-311++G(3df,3pd) basis set. SDD pseudopotentials and basis functions were used for Nb and Ta, and an all-electron basis was used for V. The bond lengths and angles are in angstroms and degrees, respectively. The electronic states are shown below the structures.

among which the dihydrido ion has a similar ring structure with C<sub>1</sub> symmetry. The C–C bond of VH<sub>2</sub>–C<sub>2</sub>H<sub>2</sub>(<sup>2</sup>A<sub>2</sub>) is the shortest among the dihydrido complexes, indicating that the C–V bonds are probably the weakest. The HMH angle gradually increases with increasing atomic weight of the metal. The two possible (C<sub>1</sub> and C<sub>s</sub>) VH–C<sub>2</sub>H<sub>3</sub> structures in their quartet states are also shown in Figure 12, and the probable Nb insertion complex also has a C<sub>1</sub> structure in the ground quartet state.

## Conclusions

Reactions of ethylene with laser-ablated group 5 metal atoms (V, Nb, and Ta) were carried out during condensation with excess argon. The matrix IR spectra and variation upon photolysis and annealing were examined. All three metals form dihydrido complexes (MH<sub>2</sub>–C<sub>2</sub>H<sub>2</sub>), which is presumably the final reaction intermediate prior to elimination of hydrogen.<sup>6,12</sup> While only the dihydrido complex is identified in the Ta spectra, V produces the insertion (VH–C<sub>2</sub>H<sub>3</sub>) as well as the dihydrido

complex, and a small amount of the Nb insertion complex is likely produced. The observed products are consistent with the predicted relative energies. The present results also suggest that the complex with metal atom in higher valence is more favored on going down the column in the periodic table, similar to the observed trend from C–H insertion reactions of CH<sub>4</sub> and CH<sub>3</sub>X with laser-ablated early transition metals.<sup>31</sup>

Experiments with CH<sub>2</sub>CD<sub>2</sub> show conclusively that the dihydrido complex is formed mostly by  $\beta$ -hydrogen transfer in the insertion complex as all three mixed H/D dihydro complexes are produced and trapped in the matrix.

We report direct observation and electronic structure calculations of MH<sub>2</sub>–C<sub>2</sub>H<sub>2</sub> and MH–C<sub>2</sub>H<sub>3</sub> complexes of group 5 metals. Strong VH<sub>2</sub> and NbH<sub>2</sub> absorptions are observed in the spectra, while no TaH<sub>2</sub> absorptions are found. Especially the VH<sub>2</sub> absorptions increase dramatically upon photolysis along with those from the dihydrido and insertion complexes. Assuming that the metal hydrides are formed by metal reaction with the released hydrogen, the observed trends for the relative yields of the primary products and metal dihydrides are consistent with the relative reaction energies in the quartet potential surface. The present results support the presumption in the reaction dynamics investigation<sup>6,12</sup> that niobium atom-induced hydrogen elimination from ethylene takes place on the quartet potential energy surface.

**Acknowledgment.** We gratefully acknowledge financial support from NSF Grant CHE 03-52487 to L.A.

**Supporting Information Available:** Figures S1 and S2, giving IR spectra and molecular structures, and Tables S1 and S2, listing IR frequencies. This material is available free of charge via the Internet at <http://pubs.acs.org>

## References and Notes

- (1) (a) Hall, C.; Perutz, R. N. *Chem. Rev.* **1996**, *96*, 3125. (b) Shilov, A. E.; Shul'pin, G. B. *Chem. Rev.* **1997**, *97*, 2879.
- (2) Jiao, C. Q.; Freiser, B. S. *J. Phys. Chem.* **1995**, *99*, 3969.
- (3) (a) Parnis, J. M. P.; Lafleur, R. D.; Rayner, D. M. *J. Phys. Chem.* **1995**, *99*, 673. (b) Thompson, M. G. K.; Parnis, J. M. *J. Phys. Chem. A* **2005**, *109*, 9465.
- (4) (a) Yi, S. S.; Blomberg, M. R. A.; Siegbahn, P. E. M.; Weisshaar, J. C. *J. Phys. Chem. A* **1998**, *102*. (b) Reichert, E. L.; Yi, S. S.; Weisshaar, J. C. *Int. J. Mass Spectrom.* **2000**, *196*, 55. (c) Wen, Y.; Poremski, M.; Ferrett, T. A.; Weisshaar, J. C. *J. Phys. Chem. A* **1998**, *102*, 8362. (d) Carroll, J. J.; Haug, K. L.; Weisshaar, J. C. *J. Am. Chem. Soc.* **1993**, *115*, 6962.
- (5) (a) Carroll, J. J.; Haug, K. L.; Weisshaar, J. C.; Blomberg, M. R. A.; Siegbahn, P. E. M.; Svensson, M. *J. Phys. Chem.* **1995**, *99*, 13955. (b) Carroll, J. J.; Weisshaar, J. C. *J. Phys. Chem.* **1996**, *100*, 12355.
- (6) (a) Stauffer, H. U.; Hinrichs, R. Z.; Schroden, J. J.; Davis, H. F. *J. Phys. Chem. A* **2000**, *104*, 1107. (b) Willis, P. A.; Stauffer, H. U.; Hinrichs, R. Z.; Davis, H. F. *J. Phys. Chem. A* **1999**, *103*, 3706.
- (7) Gidden, J.; van Koppen, P. A. M.; Bowers, M. T. *J. Am. Chem. Soc.* **1997**, *119*, 3935.
- (8) Guo, B. C.; Castleman, Jr., A. W. *Int. J. Mass Spectrom. Ion Proc.* **1992**, *113*, R1.
- (9) Sanders, L.; Hanton, S.; Weisshaar, J. C. *J. Phys. Chem.* **1987**, *91*, 5145.
- (10) Sievers, M. R.; Jarvis, L. M.; Armentrout, J. *Am. Chem. Soc.* **1998**, *120*, 1891.
- (11) Simon, A.; MacAleese, L.; Boissel, P.; Maitre, P. *Int. J. Mass Spectrom.* **2002**, *219*, 457.
- (12) Poremski, M.; Weisshaar, J. C. *J. Phys. Chem. A* **2000**, *104*, 1524.
- (13) (a) Siegbahn, P. E. M.; Blomberg, M. R. A.; Svensson, M. *J. Am. Chem. Soc.* **1993**, *115*, 1952. (b) Blomberg, M. R. A.; Siegbahn, P. E. M.; Svensson, M. *J. Phys. Chem.* **1992**, *96*, 9794. (c) Blomberg, M. R. A.; Siegbahn, P. E. M.; Yi, S. S.; Noll, R. J.; Weisshaar, J. C. *J. Phys. Chem. A* **1999**, *103*, 7254.
- (14) Rivalta, I.; Russo, N.; Sicilia, E. *J. Mol. Struct.: THEOCHEM* **2006**, *762*, 25.
- (15) Bauschlicher, C. W., Jr.; Langhoff, S. R.; Partridge, H. *J. Phys. Chem.* **1991**, *95*, 6194.
- (16) Sodupe, M.; Bauschlicher, C. W., Jr.; Langhoff, S. R.; Partridge, H. *J. Phys. Chem.* **1992**, *96*, 2118.
- (17) Lee, Y. K.; Manceron, L. *J. Phys. Chem. A* **1997**, *101*, 9650.
- (18) (a) Cho, H.-G.; Andrews, L. *J. Phys. Chem. A* **2004**, *108*, 3965 (Zr + C<sub>2</sub>H<sub>4</sub>). (b) Cho, H.-G.; Andrews, L. *J. Phys. Chem. A* **2004**, *108*, 10441 (Hf + C<sub>2</sub>H<sub>4</sub>).
- (19) Wang, G.; Chen, M.; Zhou, M. *Chem. Phys. Lett.* **2005**, *412*, 46.
- (20) (a) Zhou, M. F.; Andrews, L. *J. Phys. Chem. A* **1998**, *102*, 8251. (b) Wang, X.; Andrews, L. *J. Phys. Chem. A* **2003**, *107*, 570.
- (21) Andrews, L.; Citra, A. *Chem. Rev.* **2002**, *102*, 885 and references therein.
- (22) Frisch, M. J.; Trucks, G. W.; Schlegel, H. B.; Scuseria, G. E.; Robb, M. A.; Cheeseman, J. R.; Montgomery, J. A., Jr.; Vreven, T.; Kudin, K. N.; Burant, J. C.; Millam, J. M.; Iyengar, S. S.; Tomasi, J.; Barone, V.; Mennucci, B.; Cossi, M.; Scalmani, G.; Rega, N.; Petersson, G. A.; Nakatsuji, H.; Hada, M.; Ehara, M.; Toyota, K.; Fukuda, R.; Hasegawa, J.; Ishida, M.; Nakajima, T.; Honda, Y.; Kitao, O.; Nakai, H.; Klene, M.; Li, X.; Knox, J. E.; Hratchian, H. P.; Cross, J. B.; Bakken, V.; Adamo, C.; Jaramillo, J.; Gomperts, R.; Stratmann, R. E.; Yazyev, O.; Austin, A. J.; Cammi, R.; Pomelli, C.; Ochterski, J. W.; Ayala, P. Y.; Morokuma, K.; Voth, G. A.; Salvador, P.; Dannenberg, J. J.; Zakrzewski, V. G.; Dapprich, S.; Daniels, A. D.; Strain, M. C.; Farkas, O.; Malick, D. K.; Rabuck, A. D.; Raghavachari, K.; Foresman, J. B.; Ortiz, J. V.; Cui, Q.; Baboul, A. G.; Clifford, S.; Cioslowski, J.; Stefanov, B. B.; Liu, G.; Liashenko, A.; Piskorz, P.; Komaromi, I.; Martin, R. L.; Fox, D. J.; Keith, T.; Al-Laham, M. A.; Peng, C. Y.; Nanayakkara, A.; Challacombe, M.; Gill, P. M. W.; Johnson, B.; Chen, W.; Wong, M. W.; Gonzalez, C.; Pople, J. A. *Gaussian 03*, Revision B.04; Gaussian, Inc.: Pittsburgh, PA, 2003.
- (23) (a) Becke, A. D. *J. Chem. Phys.* **1993**, *98*, 5648. (b) Lee, C.; Yang, Y.; Parr, R. G. *Phys. Rev. B* **1988**, *37*, 785.
- (24) Andrae, D.; Haeussermann, U.; Dolg, M.; Stoll, H.; Preuss, H. *Theor. Chim. Acta* **1990**, *77*, 123.
- (25) Pople, J. A.; Krishnan, R.; Schlegel, H. B.; Binkley, J. S. *Int. J. Quant. Chem.* **1978**, *14*, 545.
- (26) Burke, K.; Perdew, J. P.; Wang, Y. In *Electronic Density Functional Theory: Recent Progress and New Directions*; Dobson, J. F., Vignale, G., Das, M. P., Eds.; Plenum: New York, 1998.
- (27) Frisch, M. J.; Head-Gordon, M.; Pople, J. A. *Chem. Phys. Lett.* **1990**, *166*, 281.
- (28) Page, M.; Doubleday, C.; McIver, J. W., Jr. *J. Chem. Phys.* **1990**, *93*, 5634.
- (29) (a) Van Zee, R. J.; Li, S.; Weltner, W., Jr. *J. Chem. Phys.* **1995**, *102*, 4367. (b) X. Wang and L. Andrews, unpublished data.
- (30) (a) Scott, A. P.; Radom, L. *J. Phys. Chem.* **1996**, *100*, 16502. (b) Andersson, M. P.; Uvdal, P. L. *J. Phys. Chem. A* **2005**, *109*, 3937.
- (31) Andrews, L.; Cho, H.-G. *Organometallics* **2006**, *25*, 4040 and references therein (review for M + CH<sub>4</sub> and CH<sub>3</sub>X).